Majoinen, Johanna; Hassinen, Jukka; Haataja, Johannes S.; Rekola, Heikki T.; Kontturi, Eero; Kostiainen, Mauri A.; Ras, Robin H A; Törmä, Päivi; Ikkala, Olli

Chiral Plasmonics Using Twisting along Cellulose Nanocrystals as a Template for Gold Nanoparticles

Published in:
Advanced Materials

DOI:
10.1002/adma.201600940

Published: 13/07/2016

Document Version
Peer-reviewed accepted author manuscript, also known as Final accepted manuscript or Post-print

Please cite the original version:
Majoinen, J., Hassinen, J., Haataja, J. S., Rekola, H. T., Kontturi, E., Kostiainen, M. A., Ras, R. H. A., Törmä, P., & Ikkala, O. (2016). Chiral Plasmonics Using Twisting along Cellulose Nanocrystals as a Template for Gold Nanoparticles. *Advanced Materials*, *28*(26), 5262–5267. https://doi.org/10.1002/adma.201600940

Chiral plasmonics using twisting along cellulose nanocrystals as a template for gold nanoparticles

Johanna Majoinen, Jukka Hassinen, Johannes S. Haataja, Heikki T. Rekola, Eero Kontturi, Mauri A. Kostiainen, Robin H. A. Ras, Päivi Törmä and Olli Ikkala**

J. Majoinen, J. Hassinen, J. S. Haataja, H. T. Rekola, Prof. R.H.A. Ras, Prof. P. Törmä, Prof. O. Ikkala
Department of Applied Physics, Aalto University, P.O. Box 15100, FIN-00076 Aalto, Espoo, Finland
E-mail: Olli.Ikkala@aalto.fi, paivi.torma@aalto.fi

Prof. E. Kontturi
Department of Forest Products Technology, Aalto University, P. O. Box 16300, FIN-00076 Aalto, Espoo, Finland

Prof. M. A. Kostiainen
Department of Biotechnology and Chemical Technology, Aalto University, P.O. Box 16100, FIN-00076 Aalto, Espoo, Finland

Keywords: cellulose nanocrystal, twisted nanorod, colloidal dispersion, templated nanoparticles, chiral plasmonics

Nanocelluloses with native crystalline internal structures have attracted considerable interest due to their plant-based origin, high mechanical properties, modifiability, and chiral liquid crystallinity, which suggest novel functional sustainable materials.[1−27] In particular, cellulose nanocrystals (CNCs) are colloidal rods, having a typical lateral dimension of 5−10 nm and length of 50−300 nm. Above a critical aqueous concentration, they exhibit left-handed chiral nematic (cholesteric) liquid crystallinity (LC) and optical iridescence,[4-6] which is preserved in dried films[4,28]. It allows templating for photonic materials using inorganics, nanoparticles, polymers, and pyrolyzed carbonized matter.[10,12,16,25,26] On the other hand, the CNCs have been suggested to possess a right-handed twist along their nanorod axis to explain the left-handed twist in their chiral LC.[6] Recently, the right-handed twist of individual CNCs and nanocelluloses of three different origins was observed by cryo-electron tomography (cryo-ET), and electron and atomic force microscopy[27,29] supported by molecular dynamics simulations[30−32].

Exploiting the twisting shape along the individual CNC nanorods could allow new optical functions in the nano/colloidal scale in dilute aqueous dispersions, i.e. not limited to the chiral LC based on the inter-rod assembly involving a larger length scale. Surprisingly, such optical findings have not been reported so far.

Surface plasmons, i.e. collective oscillations of the conduction electrons on metal surfaces, allow physics and applications ranging from photonic devices, sensing, and solar cells to pharmacology.[33−37] In nanoparticles (NPs) the oscillations become coupled to allow a chiral plasmonic response, provided that they are sufficiently closely positioned and assembled in a chiral manner. This manifests in circular dichroism (CD) spectroscopy, which describes the difference in absorption between left- and right-handed circularly polarized light. The chiral coupling of surface plasmons induces a bisignated CD signal with a zero-crossing at the characteristic localized surface plasmon resonance wavelength of the isolated NPs. Such a Cotton effect is either dip−peak or peak−dip, depending on the handedness of chirality.[38−42] In chiral biological molecules, such as DNA, proteins and polypeptides, the CD signal is at ultraviolet wavelengths, whereas the CD signal of helical metal nanoparticle assemblies is at the visible wavelengths. This extends the applications to e.g. in biosensing.[37] Chiral nanoparticle assemblies have been shown using helical polymers, supramolecular fibers, and DNA-based constructs as templates.[40−42] In particular, a chiral plasmonic signal is obtained using DNA-origami to organize the nanoparticles in well-defined helices with tunable pitch, separation, and handedness.[40,41] Even if the above approaches are promising allowing *in-depth* tunable chiral plasmonic response, introducing rapid, scalable, and economic ways for producing chiral plasmonic nano-objects is still a challenge.

Here, we explore a hypothesis whether electrostatically templating cationic gold nanoparticles (AuNPs) on the surfaces of individualized anionic CNC colloidal rods with chiral twisting along their axis allows a chiral plasmonic response in the nanoscale, i.e., without the left-handed cholesteric LC phase. The question can be put also to broader

conceptual contexts: 1) Can one physically bind plasmonic nanoparticles on colloidal rod-like templates, which, in spite of the inherent packing disorder still allows a relevant plasmonic signal; and 2) If the rod-like template shows chirality, can one break the nanoparticle packing symmetry to allow chiral plasmonics. A third aspect relates to whether electrostatic interactions can be used between the rod-like and spherical colloids without excessive aggregation. That electrostatic interactions between two colloids can be subtle, has been pointed out recently.[43]

We demonstrate that in dilute dispersions, AuNPs can be electrostatically bound on CNCs exhibiting a pronounced chiral right-handed plasmonic response, opposite to that of left-handed plasmonics of their LC assemblies, due to formation of nanoscale fibrillar CNC/AuNP superstructures. Therein, tuning of nanoparticle concentrations, sizes and charge screening is central. The CD signal is reproduced using numerical simulations utilizing the AuNP coordinates from cryo-ET.

CNCs were prepared from cotton filter paper (Whatman 1) using sulfuric acid hydrolysis[44,45], leading to anionic sulfate ester groups on their surface (**Scheme 1**). The surface charge was 0.36 eq/kg by conductometric titration as corresponding to a charge density of 0.6 e/nm^2. Cryogenic transmission electron microscopy (cryo-TEM) shows the typical rod-like appearance of the visually clear aq. dispersed CNCs (concentration 5 mg/mL), **Figure 1**a. The lateral dimension is ca. 7 nm and the lengths range from 50 to 300 nm.[27, 46] Importantly, the cellulose native crystal internal packing frustration within the CNCs (Scheme 1a) remains after sulfuric acid hydrolysis, which manifests in the chiral right-handed twisting along the CNC rods.[27,29,47]

Spherical cationized AuNPs with 11.7 ± 1.7 nm, 8.5 ± 1.2 nm and 2.6 ± 0.5 nm core sizes were synthesized (see Supporting Information), involving ligands with cationic quaternized ammonium peripheral end groups. The positive charges allow Coulombic stabilization in aqueous dispersions. The 8.5 nm and 11.7 nm AuNPs are protected by (11-

mercaptoundecyl)-*N*,*N*,*N*-trimethylammonium bromide ligands (Figure 1b) (**Table S1,** Supporting Information), as synthesized by the citrate reduction method and subsequently cationized by a two-step phase transfer method.[48] The 2.6 nm AuNPs incorporate 23-mercapto-*N*,*N*,*N*-trimethyl-3,6,9,12-tetraoxatricosan-1-aminium bromide ligands.[49] It allows a hydrodynamic size matching to the lateral dimensions of CNCs to ensure similar binding arrangement on CNCs as with AuNPs having larger cores. The core size distributions, the hydrodynamic diameters, and zeta potentials are given in **Figure S1** and **Table S1** (Supporting Information).

Templating was pursued based on the electrostatic interactions between cationic AuNPs and anionic CNCs. To suppress premature precipitation and uncontrolled aggregation, a dilute aqueous dispersion of CNC was added slowly to the AuNP aqueous dispersion, the mixture was vortex stirred between each addition (Scheme 1b), and unbound AuNPs were removed in the end by washing. We first describe the 8.5 nm AuNPs as they gave the largest CD signal upon binding on CNCs. Based on an initial screening of feasible aqueous concentrations CNC and AuNP dispersions, a fixed amount of aqueous dispersion of CNCs (1.72 mg/mL, 360 nM, 21 µL, see Supporting Information for the molarity estimation) was added dropwise to the aqueous AuNP dispersion (0.88 mg/mL, 220 nM, 1 mL). To get a rough indication of the respective amounts, these CNC and AuNP concentrations correspond to nominally ca. 30 AuNPs *vs.* each CNC. Therefore, an excess of AuNPs is suggested, as nominally ca. 15 AuNPs could be sterically fitting on the two hydrophilic facets of CNCs (see Supporting information). A visually clear colloidal dispersion was obtained after combining the two dispersions, suggesting that macroscopic aggregation was avoided. Cryo-TEM showed nanoscale objects with lateral dimensions in the scale of 30−60 nm and lengths varying from 200 to 500 nm (**Figure 2**a, **3**d), i.e., involving a few layers of CNCs and AuNPs. We denote them as CNC/AuNP fibrillar superstructures. No LC is observed due to the low concentration of CNCs. **Figures S2** and **S3** (Supporting Information) present additional cryo-

TEM images of the CNC/AuNP (8.5 nm) supracolloidal fibrillar superstructures (for electron tomogram, see **Movie S1,** Supporting Information).

The UV-vis spectra of aqueous dispersions of pure AuNPs indicate characteristic surface plasmon resonance bands at 523 nm (Figure 1c and Figure 3a). The resonance is pronounced for 8.5 nm and 11.7 nm AuNPs but strongly reduced for the 2.6 nm AuNP, due to the smaller NP core size. The pristine CNCs (0.024 mg/mL, fixed amount of CNCs added to AuNP dispersion) do not show distinguishable UV-vis signals (Figure 1c, Figure 3a). Also the CD spectra of the aqueous pristine CNCs or pristine AuNPs do not show any distinguishable signals at these concentrations (Figure 3b).

The UV-vis absorption spectrum of CNC/AuNP (8.5 nm) fibrillar superstructures in dilute aqueous medium (ρ_{CNC} = 0.01 mg/mL) shows a resonance band at 526 nm (Figure 2a, Figure 3a). The observed slight 3 nm red-shift *vs.* pure AuNPs likely originates from a change in the dielectric environment of the AuNPs upon binding onto CNC surface. The CD spectra of CNC/AuNP fibrillar superstructures consistently show a clear dip-peak bisignated signal (Figure 2a, Figure 3b). Such a spectral shape corresponds to a *right-handed* chiral assembly of the metal nanoparticles, suggesting that the AuNPs indeed adsorb to the CNC surfaces and follow their *right-handed* twisting. Note that it is opposite to the case when the chiral plasmonic signal is due to nanoparticles templated by the *left-handed* cholesteric LC phase observed at high CNC concentrations (see schematics in **Figure S7**, Supporting Information).[2,10,16,25,26]

The CNC/AuNP fibrillar superstructures render a CD signal dip-peak magnitude of 1.7 mdeg for our nominal initial aqueous CNC concentration of approximately 2.5 nM (ρ_{CNC} = 0.01 mg/mL) (Figure 3b). In comparison, DNA-origami-based right-handed assembly composed of 10 nm AuNPs exhibits a dip-peak value of 1.2 mdeg using 1.5 nM concentration of nanohelixes.[41] Therefore, the present signal is relatively large, taken our simple approach

where the NP binding on the template is controlled only statistically, i.e. not engineering specific NP binding sites on the template.

To shed light to the fibrillar superstructure assembly, the interactions, AuNP sizes and AuNP/CNC mutual amounts were explored. The right-handed CD signal diminishes to zero upon addition of NaCl due to electrostatic screening, and ultimately a complete phase separation between CNC and AuNP (8.5 nm) takes place (**Figure S4,** Supporting Information). This shows that the CD signal originates from the electrostatic binding of AuNPs on the twisted CNC rods. On the other hand, employing larger nanoparticles (core size 11.7 nm, hydrodynamic radius 15.4 nm) does not produce a well-defined CD signal (Figure 2b), which we attribute to their size mismatch to CNCs (ca. 7 nm). Using smaller 2.6 nm AuNPs produces fibrillar CNC/AuNP superstructures due to their matching hydrodynamic size, but no CD signal is observed as the nanoparticles are too small for a strong plasmon resonance (Figure 2c). Therefore, an optimal size of the nanoparticles is needed that enables chiral ordering of the nanoparticles while providing sufficiently strong plasmonic strength. A pronounced CD signal could be achieved for AuNPs with core sizes of 8.5 nm and hydrodynamic radius 12.5 nm, i.e., when the dimensions of the AuNPs and CNCs roughly match. Also the mutual amounts of AuNP (8.5 nm) and CNC were tuned, by keeping the aqueous CNC concentration fixed and modifying the AuNP aqueous concentrations from the nominally 30 AuNPs (8.5 nm) *vs.* CNC (see details in Supporting Information, **Figure S5**). Doubling the AuNP (8.5 nm) concentration leads to less-dense packing of AuNPs, reduced fibrillar aggregation, and poor CD signal. We suggest that this arises due to loosely connected cloud of AuNPs around mostly individualized CNCs, which will be removed at the final washing stage (Figure S5). On the other hand, using a half amount of AuNP (8.5 nm), CD-signal could not even be measured due to AuNP-mediated aggregation. Therefore, there exists an optimum amount of AuNP *vs.* CNC.

The formation of electrostatically bound fibrillar CNC/AuNP structures is actually not unexpected. The complex interplay of electrostatic forces between colloids[43] can allow 3D colloidal crystal, if the components are well-defined, such as cationic AuNPs with negative viruses.[48,49] Here, the formation of well-ordered 3D structures is suppressed due to the polydispersity of CNCs, thus breaking the symmetry, suggesting fibrillar CNC/AuNP-structures, as the lateral dimension of CNC is more controlled than the length.

The AuNP positions on the CNC seem quite disordered, still rendering a plasmonic CD signal. Electron tomograms[50] allow analyzing the particle-to-particle separation and the chiral component of their packing. We reconstructed the 3D positions of AuNPs (8.5 nm) of CNC/AuNP fibrillar superstructures, Figure 3d (see Supporting Information for further examples to provide statistics, **Figure S6**). The 3D positions of its 118 AuNPs were extracted from the electron tomogram data, and the calculated center-to-center nearest neighbour average distances for two AuNPs were 10.0 ± 1.8 nm, leading to the average core distance of ca. 1.5 nm (Figure 3d). Therefore, it is feasible to expect their plasmonic coupling.

Next, we simulated (Figure S6, Supporting Information) the corresponding CD response for each structure using a coupled-dipole approach.[38,39,41] The simulations (Figure 3c) capture the essential experimental observations (Figure 3b). Thus, the main contribution to the experimentally observed CD signal undeniably originates from the arrangement of the AuNPs having a slight helical asymmetry in their assembly along the CNCs. That a chiral CD signal can be observed even if the mutual distances between AuNPs are not strictly defined is also suggested by a theoretical study.[38]

In summary, a simple route for chiral plasmonics is shown by binding cationic 8.5 nm gold nanoparticles on negatively charged CNCs having a lateral dimension of ca. 7 nm and chiral twist along their rod axis dispersed in dilute aqueous medium. This leads to a bisignate CD signal indicating a right-handed chiral plasmonic response. The electrostatic self-assembly leads to nanoscale fibrillar superstructures having lateral dimensions of 30−60 nm

and length of 200−500 nm. We confirm our experimental optical results by simulating the CD signals using experimentally determined AuNP 3D coordinates from electron tomograms. The mutual sizes of CNCs and AuNPs have to match: Too large AuNPs do not effectively bind on CNCs, and too small AuNPs do not provide strong enough plasmonic signal. The present concept is fundamentally different from the previously observed left-handed chiral plasmonic responses resulting from nanoparticles embedded within chiral liquid crystalline template by CNCs. This is the first time that the chiral twist along CNC is used for a chiral plasmonic response. There exists a wealth of biological helical colloidal materials that could also allow templating of nanoparticles for chiral plasmonics. In more general, we suggest that individual chirally twisting or helical colloidal templates can lead to chiral plasmonic superstructures by utilizing supramolecular interactions, taken their concentrations, dimensions, and interaction strengths are tuned.

Acknowledgements

This work was funded by Academy of Finland by project BENMAP, the Centers of Excellence of Molecular Engineering of Biosynthetic Hybrid Materials Research and Computational Nanoscience and academy professorship (project nos. 251748, 263347). Partial funding was received from European Research Council Advanced Grants Mimefun and CODE (ERC-2013-AdG-340748-CODE). Aalto Nanomicroscopy Center is acknowledged for use of the devices. E.K. acknowledges Academy of Finland (project no. 259500).

References

[1] D. Klemm, F. Kramer, S. Moritz, T. Lindström, M. Ankerfors, D. Gray, A. Dorris, *Angew. Chem. Int. Ed.* **2011**, 50, 5438.

[2] Y. Habibi, L. A. Lucia, O. J. Rojas, *Chem. Rev.* **2010**, 110, 3479.

[3] N. Lin, J. Huang, A. Dufresne, *Nanoscale*, **2012**, 4, 3274.

[4] J. F. Revol, H. Bradford, J. Giasson, R. H Marchessault, Gray, D. G. *Int. J. Biol. Macromol.* **1992**, 14, 170.

[5] X. M. Dong, D. G. Gray, *Langmuir*, **1997**, 13, 3029.

[6] K. Fleming, D. G. Gray, S. Matthews, *Chem. Eur. J.*, **2001**, 7, 1831.

[7] J. R. Capadona, K. Shanmuganathan, D. J. Tyler, S.J. Rowan, C. Weder, *Science*, **2008**, 319, 1370.

[8] M. Pääkkö, J. Vapaavuori, R. Silvennoinen, H. Kosonen, M. Ankerfors, T. Lindström, L. A. Berglund, O. Ikkala, *Soft Matter*, **2008**, 4, 2492.

[9] M. Nogi, S. Iwamoto, A. N. Nakagaito, H. Yano, *Adv. Mater.* **2009**, 21, 1595.

[10] K.E. Shopsowitz, H. Qi, W.Y. Hamad, M.J. MacLachlan, *Nature*, **2010**, 468, 422.

[11] H. Jin, M. Pääkkö, H. Pynnönen, J. Paltakari, A. Marmur, O. Ikkala, R. H. A. Ras, *Langmuir*, **2011**, 27, 1930.

[12] H. Qi, K.E. Shopsowitz, W.Y. Hamad, M.J. MacLachlan, *J. Am. Chem. Soc.* **2011**, 133, 3728.

[13] A. Walther, J. V. I. Timonen, I. Diez, A. Laukkanen, O. Ikkala, *Adv. Mat.* **2011**, 23, 2924.

[14] M. Kettunen, R. J. Silvennoinen, N. Houbenov, A. Nykänen, J. Ruokolainen, J. Sainio, V. Pore, M. Kemell, M. Ankerfors, T. Lindström, M. Ritala, R. H. A. Ras, O. Ikkala, *Adv. Funct. Mat.* **2011**, 21, 510.

[15] S. Kumar, M. Hofmann, B. Steinmann, E. J. Foster, C. Weder, *ACS Appl. Mater. Interfaces*, **2012**, 4, 5399.

[16] J.A. Kelly, K.E. Shopsowitz, J.M. Ahn, W.Y. Hamad, M.J. MacLachlan, *Langmuir*, **2012**, 28, 17256.

[17] M.L. Hassan, C. M. Moorefield, H. S. Elbatal, G.R. Newkome, D.A. Modarelli, N.C. Romano, *Mater. Sci & Eng. B*, **2012**, 177, 350.

[18] G. Zheng, Y. Cui, E. Karabulut, L. Wågberg, H. Zhu, L. Hu, *MRS Bulletin*, **2013**, 38, 320.

[19] M. Wang, I. V. Anoshkin, A. G. Nasibulin, J. T. Korhonen, J. Seitsonen, J. Pere, E. I. Kauppinen, R. H. A. Ras, O. Ikkala, *Adv. Mat*. **2013**, 25, 2428.

[20] M. V. Biyani, E. J. Foster, C. Weder, *ACS Macro Lett.* **2013**, 2, 236.

[21] A.R. Lokanathan, A. Nykänen, J. Seitsonen, L.-S. Johansson, J. Campbell, O.J. Rojas, O. Ikkala, J. Laine, *Biomacromolecules*, **2013**, 14, 2807.

[22] T. Saito, R. Kuramae, J. Wohlert, L. A. Berglund, A. Isogai, *Biomacromolecules*, **2013**, 14, 248.

[23] A.J. Svagan, D. Busko, Y. Avlasevich, G. Glasser, S. Baluschev, K. Landfester, *ACS Nano*, **2014**, 8, 8198.

[24] J. R. McKee, E. A. Appel, J. Seitsonen, E.Kontturi, O. A. Scherman, O. Ikkala, *Adv. Funct. Mat.* **2014**, 24, 2706.

[25] A. Querejeta-Fernández, G. Chauve, M. Methot, J. Bouchard, E. Kumacheva, *J. Am. Chem. Soc.* **2014**, 136, 4788.

[26] A. Querejeta-Fernández, B. Kopera, K. S Prado, A. Klinkova, M. Methot, G. Chauve, J. Bouchard, A. S. Helmy, E. Kumacheva, *ACS Nano*, **2015**, 9, 10377.

[27] J. Majoinen, J. S. Haataja, D. Appelhans, A. Lederer, A. Olszewska, J. Seitsonen, V. Aseyev, E. Kontturi, H. Rosilo, M. Österberg, N. Houbenov, O. Ikkala, *J. Am. Chem. Soc*. **2014**, 136, 866.

[28] J. Majoinen, E. Kontturi, O. Ikkala, D. G. Gray, *Cellulose*, **2012**, 19, 1599.

[29] I. Usov, G. Nyström, J. Adamcik, S. Handschin, C. Schutz, A. Fall, L. Bergström, R. Mezzenga, *Nat. Commun*. **2015**, 6, 7564.

[30] S. Paavilainen, T. Rog, I. Vattulainen, *J. Phys. Chem. B*, **2011**, 115, 3747.

[31] Z. Zhao, O. E. Shklyaev, A. Nili, M. N. A. Mohamed, J. D. Kubicki, V. H. Crespi, L. Zhong, *J. Phys. Chem*. A **2013**, 117, 2580.

[32] J. F. Matthews, C. E. Skopec, P. E. Mason, P. Zuccato, R. W. Torget, J. Sugiyama, M. E. Himmel, J. W. Brady, *Carbohydrate Research*, **2006**, 341, 138.

[33] M. I. Stockman, *Opt. Express*, **2011**, 19, 22029.

[34] V. K. Valev, J.J. Baumberg, C. Sibilia, T. Verbiest, *Adv. Ma*ter. **2013**, 25, 2517.

[35] L. M. Liz-Marzan, *Langmuir*, **2006**, 22, 32.

[36] O. Neumann, C. Feronti, A. D. Neumann, A. Dong, K. Schell, B. Lu, E. Kim, M. Quinn, S. Thompson, N. Grady, P. Nordlander, M. Oden, N. J. Halas, *Proc. Nat. Acad. S*ci. **2013**, 110, 11677.

[37] K. Saha, S. S.Agasti, C. Kim, X. Li, V. M. Rotello, *Chem. Rev*. **2012**, 112, 2739.

[38] Z. Fan, A. O. Govorov, *J. Phys. Chem. C*. **2011**, 115, 13254.

[39] Z. Fan, A. O. Govorov, *Nano Lett*. **2010**,10, 2580.

[40] X. Shen, C. Song, J. Wang, D. Shi, Z. Wang, N. Liu, B. Ding, *J. Am. Chem. Soc*. **2012**, 134, 146.

[41] A. Kuzyk, R. Schreiber, Z. Fan, G. Pardatscher, E.-M. Roller, A.Högele, F. C. Simmel, A. O. Govorov, T. Liedl, *Nature*, **2012**, 483, 311.

[42] A. Ben-Moshe, B. M. Maoz, A. O. Govorov, G. Markovich, *Chem. Soc. Rev*. **2013**, 42, 7028.

[43] D. A. Walker, B. Kowalczyk, M. O. Cruz, B. A. Grzybowski, *Nanoscale*, **2011**, 3, 1316.

[44] X. Dong, M. J-F. Revol, D. G. Gray, *Cellulose*, **1998**, 5, 19.

[45] C. D. Edgar, D. G. Gray, *Cellulose*, **2003**, 10, 299.

[46] E. Niinivaara, M. Faustini, T. Tammelin, E. Kontturi, *Langmuir*, **2015**, 31, 12170.

[47] S. Elazzouzi-Hafraoui, Y. Nishiyama, J-L. Putaux, L. Heux, F. Dubreuil, C. Rochas, *Biomacromolecules*, **2008**, 9, 57.

[48] J. Hassinen, V. Liljeström, M. A. Kostiainen, R. H. A. Ras, *Angew. Chem. Int. Ed.* **2015**, 127, 8101.

[49] M.A. Kostiainen, P. Hiekkataipale, A. Laiho, V. Lemieux, J. Seitsonen, J. Ruokolainen, P. Ceci, *Nature Nanotech.* **2013**, 8, 52.

[50] P. Engelhardt, in *Encyclopedia of Analytical Chemistry* (Ed: R.A. Meyers) John Wiley & Sons Ltd, Chichester, **2000**, 4948.

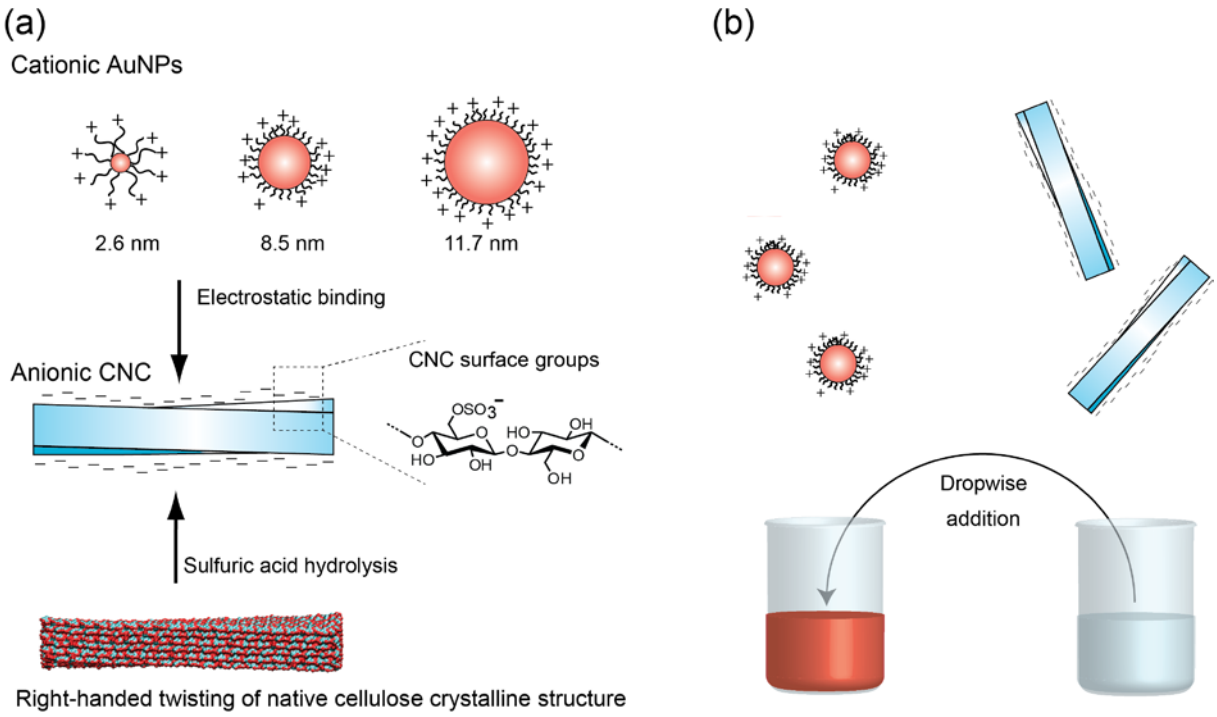

Scheme 1. Scheme for electrostatic binding of plasmonic AuNPs onto cellulose nanocrystal for chiral plasmonics in dilute aqueous dispersion. a) The native cellulose crystalline structure induces a right-handed twist (MD simulation, adapted with permission from [31]. © 2013 American Chemical Society). Upon sulfuric acid hydrolysis, rod-like CNCs with nanometer lateral dimensions show right-handed chiral twisting along the rods and anionic surface groups. b) Scheme of drop-wise adding aqueous CNC dispersion in aqueous AuNP dispersion.

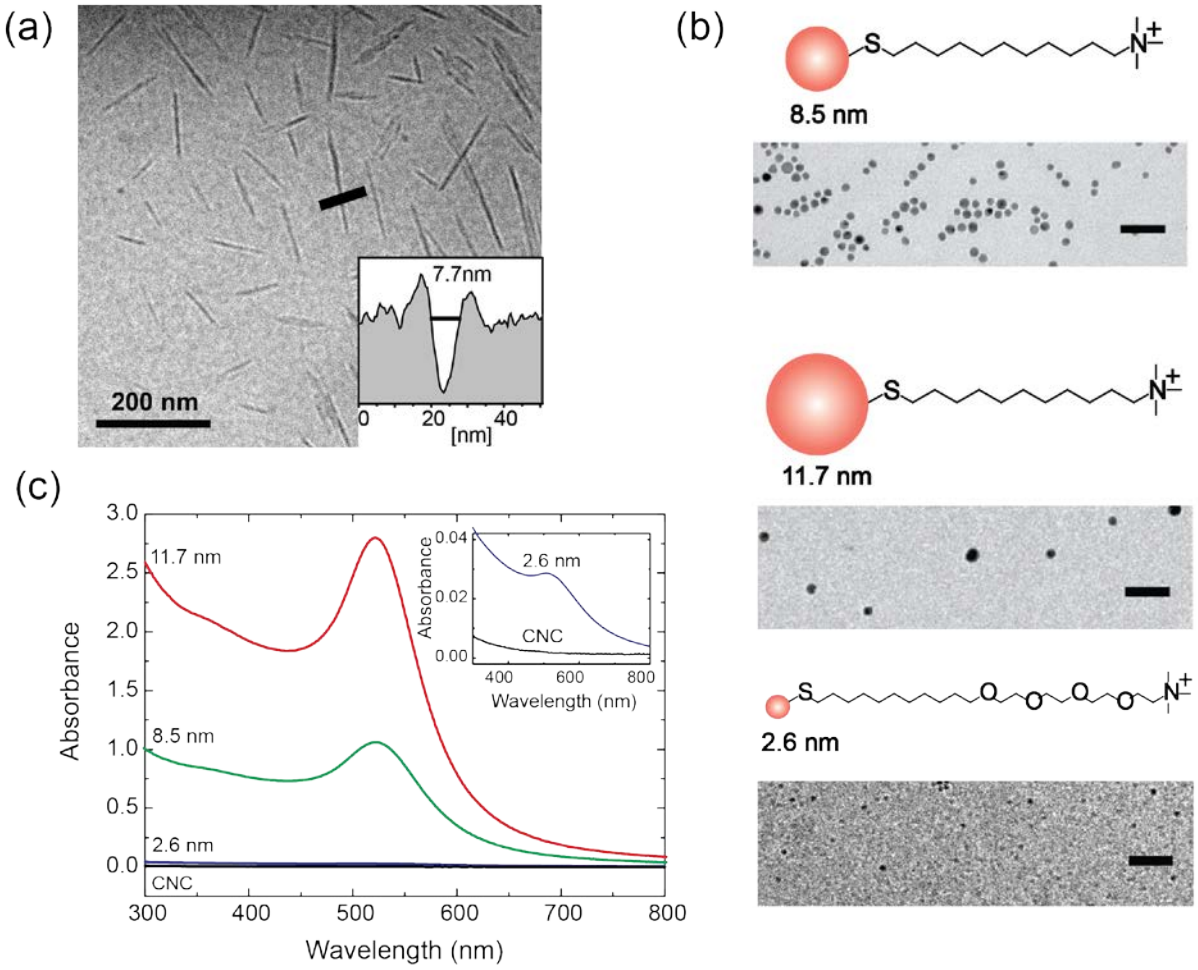

Figure 1. Starting materials. a) Cryo-TEM of pristine CNCs (5 mg/mL). b) AuNPs showing the cationic ligands, the metal core sizes, and cryo-TEM micrographs. Scale bars: 50 nm. c) UV-vis spectra of the CNCs and three different cationic AuNPs normalized to the same AuNP concentration.

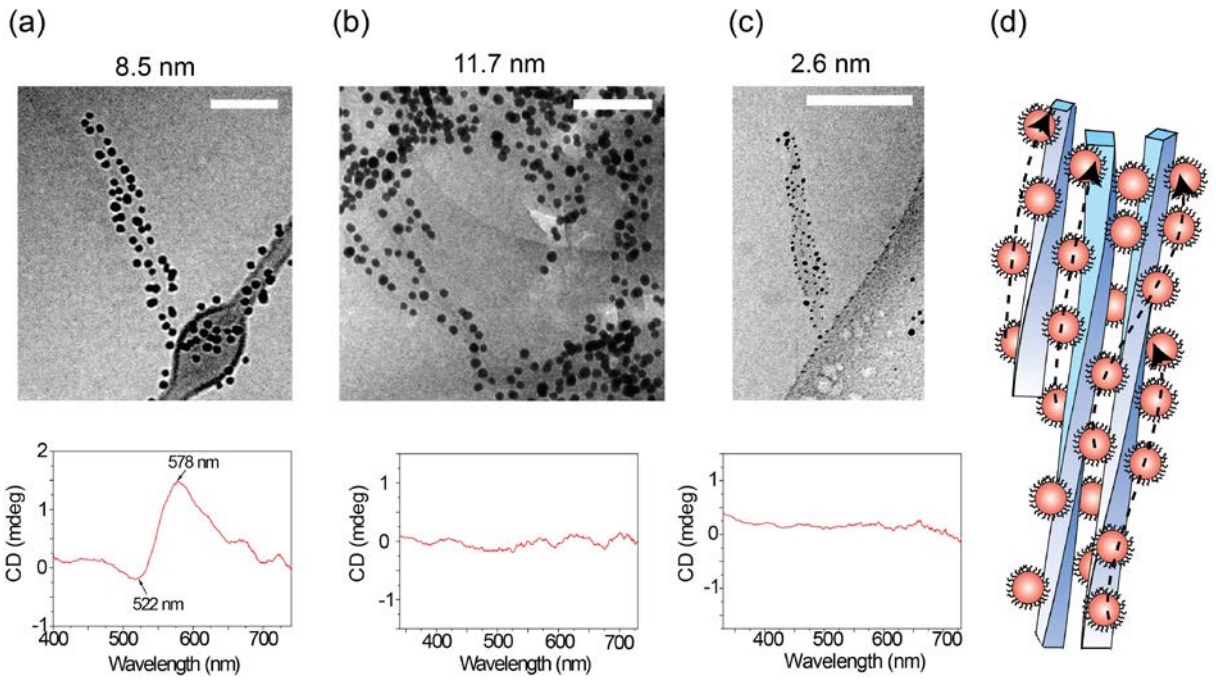

Figure 2. Cryo-TEM images and circular dichroism measurements upon electrostatic binding of AuNP onto CNC: AuNP core sizes: a) 8.5 nm, b) 11.7 nm, and c) 2.6 nm. Scale bars: 100 nm. d) The proposed scheme CNC/AuNP (8.5 nm) fibrillar superstructures, where a few anionic CNC rods with their internal right-handed chiral twisting bind positively charged AuNPs. The right-handed twisting of CNCs induces a right-handed component in the AuNP packing.

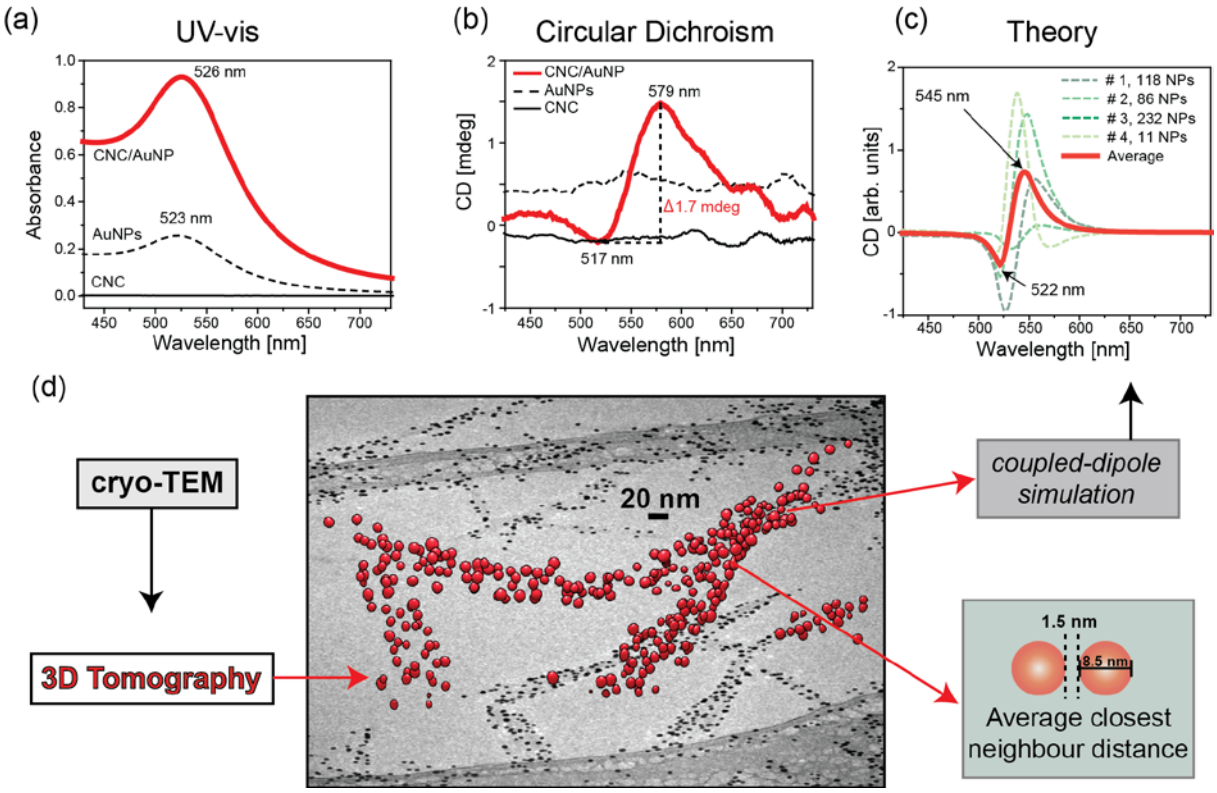

Figure 3. a) UV-Vis and b) CD spectra of CNCs, AuNPs (8.5 nm) and CNC/AuNP (8.5 nm) fibrillar superstructures. c) Simulated CD spectra for four different CNC/AuNP fibrillar superstructure tomograms (samples #1-4) taken from different positions, having different numbers of AuNPs. d) Example of cryo-ET reconstruction using 118 AuNPs (red color on top of gray-scale cryo-TEM image of the same assembly, sample sample #1, Supporting Information). The nearest neighbour distance of 1.5 nm (sample #1).

The right-handed twist along aqueous dispersed cellulose nanocrystals allows right-handed chiral plasmonics upon electrostatic binding of gold nanoparticles in dilute environment, upon tuning the particle sizes and concentrations. Simulations using nanoparticle coordinates from cryo-electron tomography confirm the experimental results. The finding suggests generalization for other chiral and helical colloidal templates for nanoscale chiral plasmonics.

Keywords: cellulose nanocrystal, twisted nanorod, colloidal dispersion, templated nanoparticles, chiral plasmonics

J. Majoinen, J. Hassinen, J. S. Haataja, H. T. Rekola, E. Kontturi, M. A. Kostiainen, R. H. A. Ras, P. Törmä* and O. Ikkala*

Chiral plasmonics using twisting along cellulose nanocrystals as a template for gold nanoparticles

ToC figure

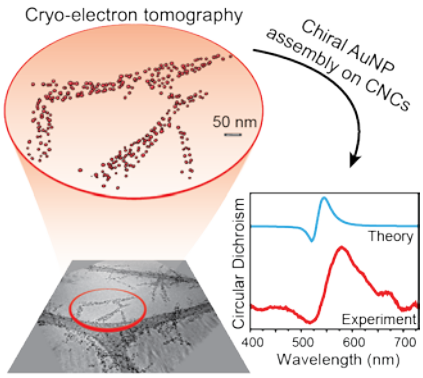

Supporting Information

Chiral plasmonics using cellulose nanocrystal twists as templates for gold nanoparticles

Johanna Majoinen, Jukka Hassinen, Johannes S. Haataja, Heikki T. Rekola, Eero Kontturi, Mauri A. Kostiainen, Robin H. A. Ras, Päivi Törmä* and Olli Ikkala*